Dynamic Alterations of Histone H3 Phospho-acetylation Correlate With Radio Sensitivity of Mitotic Cells During DNA Damage

Asmita Sharda
Advanced Centre for Treatment Research and Education in Cancer
Tripti Verma
Advanced Centre for Treatment Research and Education in Cancer
Nikhil Gadewal
Advanced Centre for Treatment Research and Education in Cancer
Sanjay Gupta (sgupta@actrec.gov.in)
Epigenetics and Chromatin Biology Group, Gupta Lab, Cancer Research Institute, Advanced Centre for Treatment, Research and Education in Cancer, Tata Memorial Centre, Kharghar, Navi Mumbai-410210,MH, India https://orcid.org/0000-0002-1209-189X

Research

Keywords: Mitosis, Histone Post Translational Modifications, DNA damage, Radiosensitivity

Posted Date: September 23rd, 2020

DOI: https://doi.org/10.21203/rs.3.rs-80009/v1

Abstract

Background - Histone Post Translational Modifications (PTMs) change in a cell cycle dependent manner and also orchestrate the DNA repair process for radiation induced DNA damage. Mitosis is the most radiosensitive phase of the cell cycle but the epigenetic events that regulate its radiosensitivity remain elusive.

Results - This study explored the dynamics between histone marks H3S10/S28ph, H3K9ac and γH2AX during mitotic DNA damage response. The presence of a mononucleosome level association between γH2AX and H3S10ph was observed only during mitosis. This association was abrogated upon cell cycle progression and chromatin de-condensation, concomitant with chromatin recruitment of DNA repair proteins Ku70 and Rad51. Moreover, the levels of H3S10/28ph remained unchanged upon DNA damage during mitosis, but decreased in a cell cycle dependent manner upon mitotic exit. However, the population that arose after mitotic progression of damaged cells comprised of binucleated tetraploid cells. This population was epigenetically distinct from interphase cells, characterized by reduced H3S10/S28ph, increased H3K9ac and more open chromatin configuration. These epigenetic features correlated with decreased survival potential of this population. The low levels of H3S10/28ph were attributed to decreased protein translation and chromatin recruitment of histone kinase Mitogen and Stress-activated Kinase 1 (MSK1) along with persistent levels of Protein phosphatase1 catalytic subunit α (PP1α).

Conclusions – This study suggests that a unique epigenetic landscape attained during and after mitotic DNA damage collectively contributed to mitotic radiosensitivity. The findings of this study have potential clinical significance in terms of tackling resistance against anti-mitotic chemotherapeutic agents.

Background

Cell cycle phase is a critical determinant of cellular radiosensitivity, with mitotic cells being most susceptible to radiation induced cell death(1–5). Fractionated irradiation regimes are designed that take advantage of mitotic radiosensitivity, and cause partial synchronization of tumor cells in mitosis to enhance cell kill(6–8). Interestingly, the DNA Damage Response (DDR) elicited by mitotic cells is unique from other cell cycle phases. A Cyclin-Dependent Kinase 1 (CDK1) regulated reversal (from prophase to interphase) is reported to occur if DNA damage is induced during late G_2 to mid prophase(9–12). However, after late prophase, priority is given to completion of cell division process over DNA repair(11). In such a situation, mitotic cells “mark” the DNA damage sites with γH2AX, Mediator of DNA Damage Checkpoint 1 (MDC1) and Mre11-Rad50-Nbs1 (MRN) complex, because CDK1 and Polo-Like Kinase (PLK1) dependent phosphorylation of p53 Binding Protein 1 (53BP1), X-ray Repair Cross Complementing protein (XRCC) and Ring Finger protein 8 (RNF8) hinders their chromatin recruitment(13–19). The recruitment of these repair proteins is initiated upon chromatin de-condensation during late telophase and G_0/G_1 phase entry, thereby completely triggering the DDR(13,20,21).

Surprisingly, DDR activation during mitosis is associated with deleterious consequences like lagging chromosomes and anaphase bridge formation(14),(22). The chromatin recruitment of 53BP1 during mitosis causes micronuclei generation, sister telomere fusion and confers a hypersensitive phenotype to mitotic cells(19). The rate of mitosis progression can also be impeded by activation of the spindle assembly checkpoint (23),(24). However, mitotic cells can bypass the spindle assembly checkpoint by Cyclin B degradation, and undergo mitotic slippage. This results in formation of tetraploid binucleated cells that arise due to cytokinesis failure. Such binucleated cells that have neither completed mitosis nor entered the G_1 phase, are called 4N-intermediate cells(25–30). Due to inter and intra-cellular heterogeneity, the fate of such cells can be either mitotic cell death or senescence. However, these cells can also re-enter the cell cycle, undergo one round of DNA replication but get arrested in the subsequent G_2 phase(31–34). However, survival and proliferation of such cells can be detrimental due to their high tumorigenic potential and drug resistant nature(35–38).

Histone Post Translational Modifications (PTMs) change according to cell cycle phases and aid in the recruitment of chromatin remodelers and repair proteins. Therefore, histone PTM alterations that occur in response to DNA damage could be a cell cycle phase specific event(39–41). Earlier studies from our group reported a dynamic kinetics of H3S10ph, observed only during the DDR of the relatively radio-resistant G_0/G_1 phase(42,43) Our recent report also indicates an association of altered histone phospho-acetylation with breast cancer radio-resistance(44). These reports suggest that a distinct interplay of H3 phospho-acetylation could regulate cell cycle phase specific radio resistance.

Keeping in mind the above propositions, this study revealed histone phospho-acetylation to be an epigenetic determinant of mitotic radiosensitivity. A mitosis-specific mononucleosome level correlation was observed between H3 phospho-acetylation and γH2AX, concomitant with negligible chromatin recruitment of DNA repair proteins. Additionally, radiated mitotic cells exhibited defects during mitotic progression and showed phenotypic variations like binucleated cells. The reduced cell survival of this population correlated with decreased H3S10/28ph, elevated H3K9ac and a de-condensed chromatin state. The H3 phosphorylation of such cells was regulated by enhanced stability of the phosphatase Protein Phosphatase 1 catalytic subunit α (PP1α) and reduced translation of Mitogen and Stress-activated Kinase 1 (MSK1) kinase. This study provides evidence of a distinct epigenetic milieu that contributes to radio-sensitivity of mitotic cells. The in-depth epigenetic analysis performed in this study can be utilized in clinics to design novel (or combinatorial) epigenetic therapies that can potentially target the surviving binucleated tetraploid cells, deemed to be tumorigenic and chemo-resistant in nature.

Results

Mitotic cells exposed to ionizing radiation (IR) exhibit G_2/M arrest, high levels of H3K9ac and reduced H3S10/28ph histone PTMs.

A time dependent analysis provided information about histone PTM alterations after mitotic DNA

ed levels of γH2AX were observed upon IR treatment while

H3S10/28ph remained unchanged (Fig. 1A and B, C-E γH2AX channel). After 2 hours of nocodazole release, more than 50% of the non-radiated cells had exited mitosis and entered the G_0/G_1 phase. However, only 30% of the radiated cells had entered the G_0/G_1 phase 4 hours after nocodazole release (Fig. 1A). This indicated that radiation exposure could lead to a delay in mitotic progression. Mitotic exit and the G_0/G_1 phase entry were marked by reduced H3S10/28ph and increased H3K9ac levels, irrespective of radiation treatment (Fig.1 A-E, Additional File 1 A-C). This was concomitant with conversion of the condensed mitotic chromatin to a de-condensed state, reminiscent of an interphase nucleus (Fig 1 C- E; DAPI channel and Additional File 1 A-C DAPI Channel).

After radiation and nocodazole release, decreased levels of γH2AX suggested ongoing repair (Fig 1B). However, there was an incremental increase in the percentage G_2/M phase cells (Fig 1A). Notably, the levels of H3S10/S28ph were neither comparable to the non-radiated cells nor increased upon G_2/M phase enrichment (Fig. 1B and Additional File 1A and B). These G_2/M enriched cells also had H3K9ac levels similar to the non-radiated cells (Fig. 1B and Additional File 1 C). Such alterations in H3S10/S28ph and H3K9ac levels also occurred irrespective of the DNA damaging agent, dose of radiation and type of cell line under study (Additional File 2 A-D). Thus, after mitotic DNA damage and cell cycle progression, a paradoxical situation existed where G_2/M phase enriched cells had low levels of mitotic marks H3S10/S28ph and increased H3K9ac.

Cellular morphology of mitotic cells after DNA damage and cell cycle progression

Contrary to the expected G_0/G_1 phase arrest, the G_2/M enrichment after mitotic exit was perplexing. Therefore, an immuno-fluorescence based analysis was performed to analyze the cellular morphology of these cells. The nuclear shape after IR and mitotic progression was distorted and fragmented, compared to well-rounded nuclei of non-radiated cells (Fig 2A, marked by red arrows). Cells exposed to IR also showed presence of micronuclei (Fig 2A, depicted by yellow arrows), chromatin-bridge (Fig. 2B marked by white arrows) and “grape phenotype” of the nuclei (Fig. 2C, represented by white arrows). Interestingly, co-incident with the previously observed G_2/M enrichment (Fig. 1A), bi-nucleated cells were detectable after IR and nocodazole release (Fig 2A, white arrows). This provided strong evidence that the previously observed G_2/M state comprised of bi-nucleated tetraploid cells, that were detected by flow cytometer to have same ploidy as the G_2/M phase.

Cell division defects in mitotic cells subjected to radiation

Live-cell microscopy was performed to analyze radiation-associated defects that could lead to the formation of bi-nucleated tetraploid cells. A significant delay in initiation of cell division was seen after IR exposure (Fig 3A white arrows in IR+ve, White arrows in 3A IR-ve also point towards cell division, quantified in 3B.). Fusion of daughter cells after cell division was also observed (Fig 3A depicted by red arrows, zoomed out figures and 3C marked by red arrow; 1h 11 min. depicts cell division and 1h 42 min. depicts cell fusion). In addition to daughter cell fusion, three distinct events were also observed when

gression. Firstly, radiated mitotic cells were able to complete

the cell division and divide into two daughter cells (Fig. 3C marked by black arrows; 0 min. is starting of time lapse and 40 min. is cell division). Secondly, cells did not initiate cell division even two hours after nocodazole release (Fig. 3C represented by blue arrows; 0 min. is starting of time lapse and 2h 50 min. represents no cell division). Thirdly, radiated cells also gave rise to asymmetric sized daughter cells (Fig. 3C depicted by green arrows, 0 min. is starting of time lapse). Therefore, radiation-associated defects in cell cycle progression mitotic cells led to the formation of unique phenotypes.

Analysis of cell cycle DNA repair and chromatin alterations in mitotic cells subjected to radiation

In context of DDR, there was no recruitment of either NHEJ specific Ku70 and HR specific Rad51 repair proteins on chromatin during mitosis (Fig. 4A). The recruitment of these proteins was concomitant with reduced γH2AX levels, observed 4 hours after nocodazole release (Fig. 4A). A comparison between the population formed after radiation and nocodazole release and an actual G_1 phase population showed cyclin B levels to be reduced but detectable upto 4 hours after IR and nocodazole release, followed by complete absence 24 hours after radiation. Additionally, IR treated population had reduced levels of cyclin D upon cell cycle progression, in comparison to non-radiated and G_0/G_1 phase cells (Fig. 4B). Additionally, MNase digestion revealed that radiated mitotic cells adopted a more de-condensed chromatin state, compared to non-radiated cells (Fig. 4E and F, points of difference marked by black arrows in 4F). Since the population generated after cell cycle progression of radiated mitotic cells was epigenetically distinct from a G_0/G_1 phase population, these cells were also assessed for their survival potential. Thus, ploidy-based Fluorescence Activated Cell Sorting (FACS) was performed to separate the G_0/G_1, S and G_2/M phase cell population 48 hours after radiation and nocodazole release (Fig. 4C). Subsequent exposure of these cell populations to IR revealed a drastic reduction in the cell survival potential, even without radiation exposure. However, it was interesting that despite a reduced survival capacity, there were some cells that were able to proliferate and produce colonies (Fig. 4D).

Histone PTMs γH2AX, H3S10/28ph and H3K9ac co-localization during mitotic DNA damage

Previous observations suggested that upon IR exposure, γH2AX and H3S10ph/S28ph co-occurred during mitosis, but not after mitotic progression (Fig 1B). This suggested an interphase specific inverse correlation between γH2AX and H3S10ph. Thus, alterations of mitotic marks H3S10/28ph were assessed during mitotic DDR. Immuno-fluorescence analysis revealed partial co-localization of γH2AX with H3S10/28ph during mitosis (seen as yellow regions). However, levels of H3K9ac in mitotic cells were too low for detection and co-localization analysis (Fig 5A-C, 0 hour time point). Interestingly, there were two striking features of cells generated after mitotic progression of radiated cells. Firstly, no co-localization was observed between γH2AX and H3S10ph, contrary to the scenario during mitosis (Fig 5A, 4 hours time point and zoomed out image). Both the histone marks were observed to form very distinct spatial foci despite being present in the same nucleus (Fig. 5A zoomed out image). Secondly, it was also apparent that cells having more intense staining of γH2AX had a dramatically reduced intensity of H3S10ph (Fig. 5A zoomed out image). H3K9ac mark was also not observed to co-localize with γH2AX (Fig. 5C zoomed

v to comment (Fig. 5B zoomed out image).

A reason for the observed co-localization between H3S10ph and γH2AX during mitosis could be the highly condensed chromatin state. The close proximity of the red and green fluorophores (representing H3S10ph and γH2AX, respectively) could lead to yellow co-localizing regions. However, upon mitotic progression and chromatin de-condensation, the fluorophores could get spatially apart, thereby causing abrogation of co-localization. Thus to ascertain whether H3S10ph and γH2AX actually co-localized during mitosis, a mono-nucleosomal co-immunoprecipitation was performed (Fig 5D and Additional File 3 A-C). Notably, both γH2AX and H3S10ph marks co-occurred on the same nucleosome during mitosis (Fig. 5D, 0 hour time point). Nucleosomes having γH2AX and H3S10ph marks also harbored H3S28ph and H3K9ac during mitosis. However, upon chromatin de-condensation, H3S10/S28ph and H3K9ac marks were absent from γH2AX-containing nucleosomes, corroborating the immunofluorescence-based observation (Fig. 5D, 4 hour time point). Interestingly, upon mitotic progression, the nucleosomes containing H3S10ph harbored H3S28ph and H3K9ac but not γH2AX. Hence, a dynamic rearrangement of chromatin upon mitotic progression led to mutual exclusion of γH2AX and H3S10ph in interphase, contrary to their co-occurrence during mitosis, corroborating our previous findings of similar nature during G_0/G_1 phase specific DDR(43).

Alterations in histone modifying enzyme levels upon mitotic DDR

Since the population generated after radiated mitotic cells that resumed cell cycle progression had reduced levels of H3S10ph, the protein levels of histone modifying kinases and phosphatases were assessed. The phosphatases Protein phosphatase1 catalytic subunit α (PP1α) and MAP Kinase Phosphatase-1 (MKP-1) showed persistent levels up to 48 and 24 hours nocodazole release, respectively. This pattern was followed irrespective of radiation treatment but with higher levels in the radiated cells (Fig. 6 A and Fig.1 A for cell cycle). Remarkably, the levels of MSK1 and Aurora Kinase B (AURKB) were reduced at 8 hours, significantly diminished at 24 hours and undetectable at 48 hours after radiation and nocodazole release. However, MSK2 levels increased after radiation and mitotic progression (Fig. 6A-B and Fig.1A for cell cycle). The non-radiated cells showed an increase in MSK1 levels 2 hours after nocodazole release, while no such increase was observed even up to 4 hours after radiation. This was a very crucial and distinguishing event between radiated and non-radiated cells. Interestingly, these time points signified the G_0/G_1 phase entry for these populations (Fig. 6A and Fig.1A for cell cycle). Apart from no induction of MSK1 protein, there was also a rapid decline in its levels. Additionally the phosphatase PP1α, but not MKP-1 showed chromatin recruitment upon mitotic progression (irrespective of radiation exposure). On the other contrary, MKP-1 was substantially enriched in the nucleo-cytoplasmic fraction (NCF) (Fig. 6D). The kinases AURKB and MSK1 also showed reduced chromatin recruitment after DNA damage and mitotic progression. The increase in H3K9ac after mitotic progression was concurrent with recruitment of histone acetyl transferases (HATs) GCN5 and PCAF on chromatin, irrespective of radiation exposure (Fig. 6D). Interestingly, reduced levels of H3S10ph and increase of H3K9ac were concomitant with chromatin recruitment of (a) HATs, (b) PP1α, and (c) reduced chromatin recruitment of HDAC1 (Fig. 6 C and D).

A previous *in silico* study from our group revealed MSK1 kinase to have a reduced affinity towards H3 peptides acetylated at positions H3K9 and K14(45). Since histone PTMs act in a combinatorial manner, the presence of a distinct set of histone PTMs could lead to an increased chromatin recruitment of a protein. Thus it was hypothesized that the acetylation on residues H3K9/K14 could lead to enhanced recruitment of phosphatase PP1α on chromatin. To investigate this, molecular modelling was performed using Swiss model software for protein structures available for PP1α and MKP-1 with a set of differentially modified histone H3 peptides (Fig 6E). The modifications on the histone peptides were H3S10ph, H3K9ac and H3K14ac in combinations of unmodified, dual and triply modified histone N-terminal tails. The calculated haddock score predicted the extent of affinity for a specific combination of phospho-acetylated H3 tail. It was observed that both MKP-1 and PP1α had comparable affinity for unmodified H3 peptides. Similar observation was seen in case of peptides having combination of only H3S10ph along with only one acetyl mark (either H3K9ac or H3K14ac). PP1α showed increased affinity for peptides having one or both H3K9ac/H3K14ac marks with absence of H3S10ph. Remarkably, this similar H3 phospho-acetyl PTM milieu was mimicked by radiated and mitosis progressed cells, with increased H3K9ac but negligible levels of H3S10ph (Fig. 6C). Therefore, these data indicated that *in silico,* the chromatin recruitment of H3 phosphatases MKP-1 and PP1α could be influenced by PTM(s) present or absent on nearby residue(s), apart from the H3S10 position.

Regulation of histone modifying kinases and phosphatases upon mitotic DNA damage and cell cycle progression

To understand the regulation of H3S10ph modifying enzymes, transcript-level alterations were analyzed in response to mitotic DDR (Fig. 7A). The transcript levels of MKP-1 and MSK1 were significantly increased 2 hours after radiation and mitotic progression while those of PP1α and AURKB were unchanged, except decreased AURKB expression 24 hours after radiation (Fig. 7A). The information provided by transcript level analysis of histone modifying kinases and phosphatases was insufficient in explaining the alterations at protein levels. This indicated that these proteins could be regulated by protein translation or degradation. Treatment of mitotic cells with protein translation inhibitor cycloheximide (CHX) did not affect mitotic progression cells, as indicated by cyclin B levels (Fig. 7B). No increase in the levels of p53 upon CHX treatment and DNA damage induction confirmed the activity of CHX. The level of MSK1 protein increased 6 hours after nocodazole release in the non-radiated cells. Such an induction was not observed upon CHX treatment, irrespective of radiation exposure. This suggested MSK1 protein levels were regulated by translation of its mRNA upon mitotic progression. Hence despite transcriptional up-regulation, there was no increase in MSK1 protein levels due to radiation induced translation-related defects. The phosphatase MKP-1 followed a cyclical pattern of increase of protein levels at 2 hours, followed by a reduction at 6 hours after radiation. These alterations at the protein levels were concomitant with the transcript level alterations Upon CHX treatment, the MKP-1 protein levels diminished, thereby suggesting MKP-1 was regulated by both transcription and translation (Fig. 7 A and B). Interestingly, the protein levels of PP1α were increased even upon CHX treatment, with unchanged transcript levels. These data indicated that protein stabilization could play an important role

In contrast to the other chromatin modifying enzymes, the protein level of AURKB declined irrespective of radiation and CHX treatment. This pointed towards the role of protein degradation in regulation of AURKB levels. Mitotic cells treated with velcade, an inhibitor of the proteasome machinery, showed sustained levels of cyclin B and AURKB (Fig. 7C). Conversely, untreated mitotic cells progressed to G_0/G_1 phase showed reduced protein levels of AURKB and cyclin B. This indicated that AURKB protein levels were regulated by proteasome-mediated degradation upon mitotic exit and interphase entry. Additionally, inhibition of protein degradation was unable to rescue the levels of MSK1 kinase, thereby indicating protein translation to be the regulator of MSK1 protein levels upon mitotic progression. In context of the phosphatases, minor accumulation of MKP-1 protein was observed upon velcade treatment and radiation exposure, thereby implying the turnover of MKP-1 to be regulated by its degradation also. Strangely, PP1α levels remained unchanged upon both protein translation and degradation inhibition. This strongly pointed towards involvement of PTM-associated protein stabilization (of PP1α or its associated regulatory subunit). Thus, the non-recovery of H3S10ph after mitotic DNA damage was a result of reduced translation of the kinase MSK1 or persistent presence of phosphatases MKP-1 and PP1α.

Discussion

Interphase, comprising of G_1, S and G_2 phases, is the longest part of the cell cycle and the DDR events associated with it are well elucidated. The emphasis of this study was to understand regulation of histone H3 phospho-acetylation during mitotic DDR. We report a mitosis specific mononucleosome level association of H3S10ph and γH2AX that is abrogated upon interphase entry and unique cellular phenotypes that arise after mitotic DNA damage as a consequence of radiation exposure. Such cells have decreased survival potential and a distinct epigenetic profile. The reduced H3S10/28ph level in these cells was contributed by decreased protein translation and chromatin recruitment of Msk1 kinase and enhanced stability of phosphatase PP1α.

The interest in H3S10ph and its nearby acetyl mark(s) originates from our previous reports about association of H3 phospho-acetylation with G_0/G_1 phase specific DDR and radio-resistance(42–44). However, the role of H3S10ph during mitotic DDR is not well explored. Our data for cell-cycle dependent reduction of H3S10/28ph upon mitotic progression and co-occurrence of these marks with γH2AX are in complete agreement with a previous study (46). Also in corroboration with a previous report, we observed reduced levels of H3K9ac during mitosis that increased upon mitotic exit (47). This was attributed to chromatin recruitment of Histone Acetyl Transferases (HATs) Gcn5 and PCAF. However, our data does not suggest DNA damage associated decrease of H3K9ac during mitotic DDR and nocodazole release(46). Several factors such as duration of nocodazole treatment, specific time point analysis after interphase entry, cell line and extent of DNA damage often lead to such contrasting observations, that reflects the dynamic nature of DDR associated epigenetic alterations(48).

Perhaps the most confounding observation of the study was the G_2/M arrest of IR exposed mitotic cells. This was actually a technical limitation of flow cytometry based cell cycle analysis, which detected bi-

nucleated tetraploid cells as G_2/M phase cells. Absence of cyclin B and reduced cyclin D levels has been reported for cells that aborted mitosis but were unable to enter the G_1 phase(33). Our live cell analysis suggests that such a “4N-intermediate” / bi-nucleated tetraploid population could also arise due to daughter cell fusion. However, further studies are required to understand radiation-associated defects in the cytokinesis process that leads to formation of bi-nucleated tetraploids.

Notably, a mixed population, comprising of G_0/G_1, S and G_2/M phase cells was generated after IR exposure to mitotic cells. Such a population could arise due to (a) normal cell cycle progression after DNA repair, (b) activation of interphase DNA damage checkpoints or (c) re-entry of binucleated cells into cell cycle. This phenotypic variability is reported to arise due to a competition between independent networks of cell survival and cell death, leading to intra-cell variation(31). Most remarkably, radiated mitotic cells adopted a more de-condensed chromatin configuration after cell cycle progression, which correlated with their reduced cell survival. This observation is in complete concordance with our recent report that suggests increased heterochromatinization upon acquirement of radio-resistance(44). Hence, these data strongly indicate that global chromatin configuration plays an essential role in determining cell fate towards radiation induced DNA damage. However, our interpretation is based on a collective analysis of diverse cell types formed after mitotic progression. Hence studies utilizing a single-cell based approach to elucidate the “cause or consequence” of a specific phenotype are essential. Ongoing studies are also aimed at understanding how H3S10/28ph and H3K9ac could affect the transcriptome of binucleated tetraploid cells that tips the scales in favor cell death or survival.

A fine balance between the levels, activity and spatio-temporal regulation of chromatin modifying enzymes maintains the equilibrium of histone phospho- acetylation. According to our *in silico* and biochemical analysis, we propose that increased histone acetylation positively influences PP1α chromatin recruitment. This was found to be in agreement with a report that suggested enhanced chromatin recruitment of PP1δ upon histone acetylation induction during mitosis(49). Further, the plausible causes of reduced H3S10ph after radiation and mitotic exit were decreased MSK1 kinase levels and persistent presence of PP1α phosphatase. A hypothesis that emerges from these data suggests that histone hyperacetylation-associated chromatin recruitment of PP1α could regulate activity of the kinase(s). While hypo-acetylated histone tails were found to be preferred substrates for AURKB mediated mitotic H3S10ph(50), it was also reported that presence of PP1 negatively regulates the kinase activity of AURKB in *Xenopus* interphase chromatin extracts(51). Most interestingly, our data suggests PP1α chromatin recruitment to occur irrespective of radiation exposure. So how does PP1α regulate kinase activity in interphase cells that arise after mitotic radiation? There can be two plausible explanations that shed light on this proposition. Firstly, the kinase activity of MSK1 is regulated by auto-phosphorylation and $ERK_{1/2}$ or p38 mediated phosphorylation(52). Therefore it could be possible that PP1α regulates either an upstream activator of MSK1 or directly the kinase. Secondly, the substrate specificity of PP1 catalytic subunit depends on its association with different regulatory subunits. Association of PP1γ with Repo-Man has been reported to regulate histone de-phosphorylation that occurs upon mitosis to G_1 transition(53,54). Formation of similar complex by PP1α could also regulate MSK1 kinase activity during

interphase, in response to DNA damage. Possibly PP1 could associate with a unique regulatory subunit upon radiation treatment, which directs its specificity towards interphase kinases. These are interesting possibilities that can bring to light the complexity of kinase-phosphatase regulation during mitotic DDR.

In context of mitotic DDR, our data suggests co-occurance of γH2AX and H3S10ph on the same mononucleosome during mitosis but not interphase. This was concomitant with an independent observation of Ku70 and Rad51 chromatin localization only upon mitotic exit. Our previous report also suggests G_0/G_1 phase specific H3S10ph decrease to be crucial for DNA repair(43),(42). This suggests that the mono-nucleosomal co-existence of H3S10ph and γH2AX might not provide a permissive environment for initiation of DNA repair during mitosis. There are four probable possibilities that led us to this conclusion. Firstly, H3S10ph is associated with DNA-RNA hybrid R-loop formation that is conserved across yeast, nematode and human cells(55). Hence, dynamic alterations of H3S10ph during mitotic DDR could be detrimental to genome stability by formation of such structures during cell division process. Secondly, it is elusive whether γH2AX-H3S10ph form homotypic or heterotypic nucleosomes. This could lead to nucleosome architecture alterations, which might hinder chromatin recruitment of remodeling factors required during DNA repair. This proposition seems plausible since structural alteration of chromatin by remodeling complexes, especially when the cell is preoccupied with the division process, might lead to genomic instability. Additionally, to further explore this possibility, it needs to be ascertained whether H3S10ph- γH2AX containing nucleosomes are present at the DNA damage site/DSB or in its vicinity. Thirdly, the activity, levels, spatio-temporal presence and accessibility of the H3S10ph and γH2AX modifying kinases and phosphatases could also govern their co-occurance. Finally, is possible that apart from H3S10ph and γH2AX, presence or absence of other PTMs is required for mitotic DNA-damage response activation, and such a milieu is attained upon chromatin de-condensation in G_1 phase. This hypothesis is based on a report by Clouaire *et. al.* that uses artificial double strand break (DSB) induction for elucidation of the histone PTM milieu around the break site(56). A similar analysis of the histone PTMs adjoining the DSBs during mitotic DDR could provide strong evidence of a “code” required to halt DDR in mitosis but initiate it in interphase.

Our study strongly suggests that key epigenetic differences between mitotic and interphase cells could lead to differences in their DDR. The report also suggests that the radio-sensitivity of mitotic cells is contributed by the epigenetic state of the population that arises after damaged mitotic cells resume cell cycle (Fig. 8). It is interesting to note tetraploid cells are tumorigenic in nature, so their survival and proliferation could lead to tumor relapse even after successful radiation regime. Therefore, an understanding of the epigenetic features of such cells could open up avenues for utilization of next-generation mitotic inhibitor therapy or combinatorial therapies with HDAC inhibitors to target the residual detrimental population.

Materials And Methods

Cell culture, synchronization: MCF7 cell line was a kind gift by Dr. Santosh Kumar Sandur, BARC, India. irsat, ACTREC and AGS cell line was purchased from ATCC.

MCF7 and U87 cells were cultured in DMEM (Invitrogen, USA) media while RPMI (Invitrogen, USA) was used for AGS cell line. The medium was supplemented with 2mM glutamine (Sigma, USA), 10% fetal bovine serum (Gibco, USA). Cell were maintained at 37°C and 5% CO_2. Synchronization in G_0/G_1 phase of the cell cycle was done by serum starvation using 0.02% serum for 72 hours. Serum starvation was stopped by adding 10% FBS containing medium 6 hours before radiation to allow cells to enter G_1 phase. Synchronization in pro-metaphase was performed by incubating cells with 200ng/ml nocodazole for 18 hours.

Nocodazole release of mitotic cells and inhibitor/drug treatment- Nocodazole release of mitotic cells was performed by shake off method(57,58). Mitotic cells were subjected to radiation while the medium still contained nocodazole. Immediately after irradiation, mitotic cells were collected by gently tapping the plates to dislodge mitotic cells. The mitotic cells collected in the medium were pelleted by centrifugation at 3000 rpm for 2 minutes at 4°C. Nocodazole (Sigma, USA) containing medium was discarded and cells washed once with 1X PBS to remove residual nocodazole and centrifuged as described above. The mitotic cells were re-suspended in nocodazole free medium and seeded into fresh 100mm^2 culture plates to allow mitotic progression. Cycloheximide (Sigma, USA) (50µg/ml) and proteasome inhibitor velcade (1µM/ml) were added 1 hour before radiation treatment and also after nocodazole release in the necessary controls. Drug treatment was given as Cisplatin (Sigma, USA) (2µg/ml for 4 hours), Ultra Violet (10J/m^2 for 15 minutes) rays, Adriamycin (Sigma, USA) (10µg/ml for 4 hours) and H_2O_2 (Sigma, USA) (500µM for 15 minutes).

Cell irradiation: A Co-60 radioactive source present in Bhabhatron-II (Panacea Medical Technologies Ltd. and Bhabha Atomic Research Centre (BARC), India) installed at the Department of Radiation Oncology, ACTREC was used to subject the cells to ionizing radiation. Field size was 25cm x 25cm, Source-to-skin distance (SSD) as 80cm and gantry was angled at 180° to the specimen.

Histone Isolation and total cell lysate preparation: Histone isolation was performed as described earlier (43). The chromatin bound histones were extracted using acid extraction method. The histones obtained in the final pellet was resuspended in 0.1% β-mercaptoethanol (Sigma, USA) and stored in -20°C. Total cell lysates were prepared by sonication of the cell pellet in the buffer described above and cleared of debris by centrifugation at 17000rpm for 30 mins at 4°C. The supernatant obtained was used as total cell lysate.

Western blotting: Histones and total cell lysates were resolved on 18% and 10% SDS-Poly-Acrylamide Gel Electrophoresis (SDS-PAGE) respectively, transferred on PVDF membrane (Immobillion) and subjected to western blotting. List of antibodies used in the study is provided in Table 1.

Immunofluorescence Microscopy- Immunofluorescence was performed as described previously (43). Imaging was done using Zeiss 510 Meta confocal microscope. Image analysis was performed using FIJI software.

Live cell imaging and analysis -

MCF7 cells were synchronized in pro-metaphase by nocodazole arrest in a glass-bottomed plate. Immediately after radiation, nocodazole-containing medium was discarded and cells were carefully washed twice with 1X PBS. Nocodazole-free medium was added to the plate and imaging was initiated. Cells were maintained at 95% relative humidity and 5% CO_2 for 3 hours during imaging process. Imaging was performed on Leica SP8 confocal microscope at 63X magnification. Images were processed using the Leica LASX software.

Flow cytometry based cell cycle analysis and sorting: Cell cycle analysis was carried out using propidium iodide (Sigma, USA) based DNA content analysis as described previously (43). DNA content analysis was carried out using Fluorescence-Activated Cell Sorting (FACS) Calibur flow cytometer (Becton Dickinson) and analysis done using MODFIT software by Verity house. Cell sorting was performed using VYBRANT green dye (Invitrogen, USA), as per manufacturer's instructions.

Clonogenic assay: MCF7 cells sorted after VYBRANT dye treatment were counted and seeded in 6 well plates. 1000 cells were seeded per well, per cell cycle phase. Cells were irradiated and maintained for 14 days. Colonies were fixed with 4% paraformaldehyde for 20 mins followed by washing with Phosphate Buffered Saline (PBS). Staining was performed using 0.5% crystal violet(59).

Cellular fractionation: Cellular fractionation into cytoplasmic, nuclear and chromatin fractions was performed as described previously(43). The nuclear and cytoplasmic fractions were pooled together to form nucleo-cytoplasmic fraction. It should be noted that western blots depicted in Fig. 4A and 7D are a part of the same experiment but depicted as separate figures. They are derived from the same experimental nucleo-cytoplasmic and chromatin lysates; hence have same histone H3 and GAPDH loading control blots.

Mono-nucleosomal Immunoprecipitation

Isolation of mono-nucleosomes was performed as previously described(43). Mono-nucleosome isolation from mitotic nuclei was done in MNase digestion buffer containing 10mM $CaCl_2$. Mono-nucleosomes were prepared by incubating 1mg chromatin with 200 units of MNase (UBS, USA) for 30 minutes at 37°C. 200µg of chromatin was incubated with 2µg of anti- γH2AX, anti- H3S10ph and IgG antibodies. 20µl of magnetic DYNA beads (Thermo Fischer, USA) were added to chromatin-antibody mixture and incubated for 4 hours on a rotating platform. Separation of antibody-nucleosome complex and washing of bound complex was done using magnetic rack. 2X SDS loading dye was added to the bead bound complex. The samples were boiled, chilled and loaded on 18% SDS-PAGE gel, followed by western blotting with respective antibodies.

Molecular homology modelling – *In silico* modelling of MKP1 and PP1α with differentially modified H3 peptides was performed as previously described(45).

Quantitative PCR: RNA extraction from was done by Trizol method, followed by DNaseI treatment (Fermentas, USA) and cDNA synthesis using random hexamer primers (Revert-Aid cDNA Synthesis Kit, Thermo Scientific, USA), strictly as per manufacturer's instructions. Real-time PCR was performed using gene specific primers using amplification conditions of 30 seconds at 94°C, 1 minute at 60°C and 1 minute at 72°C for 30 cycles followed by 10 minute final extension. List of primers used in the study is provided in Table 2. The expression of change upon radiation was plotted as fold change normalized to non-radiated cells of the indicated time points.

Statistical analysis - All numerical data were expressed as average of values obtained ± standard deviation (SD). Statistical significance was determined by conducting unpaired students *t*-test.

Declarations

Ethics approval and consent to participate

Not applicable

Consent for publication

The paper was critically read by all authors and approved for publication.

Availability of data and materials

The data in manuscript is available

Competing interests

The authors declare no competing interests.

Funding:

The authors would like to thank Advanced Centre for Treatment Research and Education in Cancer (ACTREC) – India and Department of Science and Technology (DST) - India for funding Gupta Laboratory.

Author contributions

SG and AS contributed to the conception and design of experiments. AS performed the experiments. NG performed *in silico* molecular modelling and its analysis. TV performed real-time PCR of chromatin modifying kinases and phosphatases and its data analysis. AS and SG wrote the manuscript.

Acknowledgments

The authors would like to thank the Department of Radiation Oncology, Flow cytometry and Microscopy

for her doctoral fellowship. TV is supported by ACTREC for

her doctoral fellowship. We are also thankful to Dr. Sorab Dalal, Dr. Sudeep Gupta and Dr. Prasanna Venkatraman, ACTREC for providing cyclin B antibody, VYBRANT reagent and p53 antibody, respectively.

References

1. Terasima T, Tomlach LJ. Changes in X-ray Sensitivity of HeLa Cells during the Division Cycle. Nature. 1961;190(4782):1210–1.
2. Sinclair WK, Morton RA. X-ray and ultraviolet sensitivity of synchronized chinese hamster cells at various stages of the cell cycle. Biophysical journal. 1965 Jan;5(1):1–25.
3. Terasima T, Tomlach LJ. Variations in several responses of HeLa cells to x-irradiation during the division cycle. Biophysical journal. 1963 Jan;3(1):11–33.
4. Pawlik TM, Keyomarsi K. Role of cell cycle in mediating sensitivity to radiotherapy. International Journal of Radiation Oncology*Biology*Physics. 2004;59(4):928–42.
5. Stobbe CC, Park SJ, Chapman JD. The radiation hypersensitivity of cells at mitosis. International Journal of Radiation Biology. 2002 Jan 1;78(12):1149–57.
6. Steel GG, McMillan TJ, Peacock JH. The 5Rs of radiobiology. International journal of radiation biology. 1989 Dec;56(6):1045–8.
7. Withers HR. Cell Cycle Redistribution as a Factor in Multifraction Irradiation. Radiology. 1975 Jan 1;114(1):199–202.
8. Withers HR. Radiation biology and treatment options in radiation oncology. Cancer research. 1999 Apr;59(7 Suppl):1676s–1684s.
9. Carlson JG. X-ray-induced prophase delay and reversion of selected cells in certain avian and mammalian tissues in culture. Radiation research. 1969 Jan;37(1):15–30.
10. Carlson JG. A detailed analysis of x-ray-induced prophase delay and reversion of grasshopper neuroblasts in culture. Radiation research. 1969 Jan;37(1):1–14.
11. Rieder CL, Cole RW. Entry into mitosis in vertebrate somatic cells is guarded by a chromosome damage checkpoint that reverses the cell cycle when triggered during early but not late prophase. The Journal of cell biology. 1998 Aug;142(4):1013–22.
12. Chow JPH, Siu WY, Fung TK, Chan WM, Lau A, Arooz T, et al. DNA damage during the spindle-assembly checkpoint degrades CDC25A, inhibits cyclin-CDC2 complexes, and reverses cells to interphase. Molecular biology of the cell. 2003/07/25. 2003 Oct;14(10):3989–4002.
13. Giunta S, Belotserkovskaya R, Jackson SP. DNA damage signaling in response to double-strand breaks during mitosis. The Journal of cell biology. 2010 Jul 26;190(2):197–207.
14. Terasawa M, Shinohara A, Shinohara M. Canonical Non-Homologous End Joining in Mitosis Induces Genome Instability and Is Suppressed by M-phase-Specific Phosphorylation of XRCC4. PLOS Genetics. 2014 Aug 28;10(8):e1004563.
15. Lee D-H, Acharya SS, Kwon M, Drane P, Guan Y, Adelmant G, et al. Dephosphorylation Enables the DNA Breaks. Molecular Cell. 2014;54(3):512–25.

16. Benada J, Burdová K, Lidak T, von Morgen P, Macurek L. Polo-like kinase 1 inhibits DNA damage response during mitosis. Cell cycle (Georgetown, Tex). 2015;14(2):219–31.
17. van Vugt MATM, Gardino AK, Linding R, Ostheimer GJ, Reinhardt HC, Ong S-E, et al. A mitotic phosphorylation feedback network connects Cdk1, Plk1, 53BP1, and Chk2 to inactivate the G(2)/M DNA damage checkpoint. PLoS biology. 2010 Jan 26;8(1):e1000287–e1000287.
18. Zhang W, Peng G, Lin S-Y, Zhang P. DNA damage response is suppressed by the high cyclin-dependent kinase 1 activity in mitotic mammalian cells. The Journal of biological chemistry. 2011/08/30. 2011 Oct 14;286(41):35899–905.
19. Escribano-Diaz C. Mitosis Inhibits DNA Double-Strand Break Repair to Guard Against Telomere Fusions. 2014;3–8.
20. Giunta S, Jackson SP. Give me a break, but not in mitosis: the mitotic DNA damage response marks DNA double-strand breaks with early signaling events. Cell cycle (Georgetown, Tex). 2011/04/15. 2011 Apr 15;10(8):1215–21.
21. Ciccia A, Elledge SJ. The DNA Damage Response : Making it safe to play with knives. 2011;40(2):179–204.
22. Bakhoum SF, Kabeche L, Murnane JP, Zaki BI, Compton DA. DNA-damage response during mitosis induces whole-chromosome missegregation. Cancer discovery. 2014/08/08. 2014 Nov;4(11):1281–9.
23. Smits VA, Klompmaker R, Arnaud L, Rijksen G, Nigg EA, Medema RH. Polo-like kinase-1 is a target of the DNA damage checkpoint. Nature cell biology. 2000 Sep;2(9):672–6.
24. Mikhailov A, Cole RW, Rieder CL. DNA Damage during Mitosis in Human Cells Delays the Metaphase/Anaphase Transition via the Spindle-Assembly Checkpoint. Current Biology. 2002;12(21):1797–806.
25. Brito DA, Rieder CL. Mitotic checkpoint slippage in humans occurs via cyclin B destruction in the presence of an active checkpoint. Current biology : CB. 2006 Jun 20;16(12):1194–200.
26. Lanni JS, Jacks T. Characterization of the p53-dependent postmitotic checkpoint following spindle disruption. Molecular and cellular biology. 1998 Feb;18(2):1055–64.
27. Andreassen PR, Lohez OD, Lacroix FB, Margolis RL. Tetraploid state induces p53-dependent arrest of nontransformed mammalian cells in G1. Molecular biology of the cell. 2001 May;12(5):1315–28.
28. Borel F, Lohez OD, Lacroix FB, Margolis RL. Multiple centrosomes arise from tetraploidy checkpoint failure and mitotic centrosome clusters in p53 and RB pocket protein-compromised cells. Proceedings of the National Academy of Sciences. 2002 Jul 23;99(15):9819 LP-9824.
29. Rieder CL, Maiato H. Stuck in Division or Passing through: What Happens When Cells Cannot Satisfy the Spindle Assembly Checkpoint. Developmental Cell. 2004;7(5):637–51.
30. Andreassen PR, Lacroix FB, Lohez OD, Margolis RL. Neither p21WAF Nor 14-3-3σ Prevents G2 Progression to Mitotic Catastrophe in Human Colon Carcinoma Cells after DNA Damage, But p21WAF1 Induces Stable G1Arrest in Resulting Tetraploid Cells. Cancer Research. 2001 Oct

31. Gascoigne KE, Taylor SS. Cancer Cells Display Profound Intra- and Interline Variation following Prolonged Exposure to Antimitotic Drugs. Cancer Cell. 2008;14(2):111–22.
32. Uetake Y, Sluder G. Cell cycle progression after cleavage failure: mammalian somatic cells do not possess a “tetraploidy checkpoint” . Journal of Cell Biology. 2004 Jun 7;165(5):609–15.
33. Mantel C, Guo Y, Lee MR, Han M-K, Rhorabough S, Kim K-S, et al. Cells enter a unique intermediate 4N stage, not 4N-G1, after aborted mitosis. Cell Cycle. 2008 Feb 15;7(4):484–92.
34. Panopoulos A, Pacios-Bras C, Choi J, Yenjerla M, Sussman MA, Fotedar R, et al. Failure of cell cleavage induces senescence in tetraploid primary cells. Molecular biology of the cell. 2014/08/20. 2014 Oct 15;25(20):3105–18.
35. Olaharski AJ, Sotelo R, Solorza-Luna G, Gonsebatt ME, Guzman P, Mohar A, et al. Tetraploidy and chromosomal instability are early events during cervical carcinogenesis. Carcinogenesis. 2005 Aug 19;27(2):337–43.
36. Fujiwara T, Bandi M, Nitta M, Ivanova E V, Bronson RT, Pellman D. Cytokinesis failure generating tetraploids promotes tumorigenesis in p53-null cells. Nature. 2005 Oct;437(7061):1043—1047.
37. Panvichian R, Orth K, Day ML, Day KC, Pilat MJ, Pienta KJ. Paclitaxel-associated Multimininucleation Is Permitted by the Inhibition of Caspase Activation: A Potential Early Step in Drug Resistance. Cancer Research. 1998 Oct 15;58(20):4667 LP-4672.
38. Habu T, Matsumoto T. p31comet inactivates the chemically induced Mad2-dependent spindle assembly checkpoint and leads to resistance to anti-mitotic drugs. SpringerPlus. 2013;2(1):562.
39. Soria G, Polo SE, Almouzni G. Prime, repair, restore: the active role of chromatin in the DNA damage response. Molecular cell. 2012 Jun 29;46(6):722–34.
40. Kim JJ, Lee SY, Miller KM. Preserving genome integrity and function: the DNA damage response and histone modifications. Critical Reviews in Biochemistry and Molecular Biology. 2019 May 4;54(3):208–41.
41. van Attikum H, Gasser SM. The histone code at DNA breaks: a guide to repair? Nature Reviews Molecular Cell Biology. 2005 Sep 15;6:757.
42. Sharma AK, Khan SA, Sharda A, Reddy DV, Gupta S. MKP1 phosphatase mediates G1-specific dephosphorylation of H3Serine10P in response to DNA damage. Mutation Research - Fundamental and Molecular Mechanisms of Mutagenesis. 2015;778.
43. Sharma AK, Bhattacharya S, Khan SA, Khade B, Gupta S. Dynamic alteration in H3 serine 10 phosphorylation is G1-phase specific during ionization radiation induced DNA damage response in human cells. Mutation Research/Fundamental and Molecular Mechanisms of Mutagenesis. 2015;773:83–91.
44. Sharda A, Rashid M, Shah SG, Sharma AK, Singh SR, Gera P, et al. Elevated HDAC activity and altered histone phospho-acetylation confer acquired radio-resistant phenotype to breast cancer cells. Clinical Epigenetics. 2020;12(1):4.
45. Sharma AK, Mansukh A, Varma A, Gadewal N, Gupta S. Molecular Modeling of Differentially ed lysine 9/14 of Histone H3 Regulates their Interactions with

14-3-3ζ, MSK1, and MKP1. Bioinformatics and biology insights. 2013 Aug 26;7:271–88.

46. Tjeertes J V, Miller KM, Jackson SP. Screen for DNA-damage-responsive histone modifications identifies H3K9Ac and H3K56Ac. The EMBO Journal. 2009;28(13):1878–89.
47. Kruhlak MJ, Hendzel MJ, Fischle W, Bertos NR, Hameed S, Yang X-J, et al. Regulation of Global Acetylation in Mitosis through Loss of Histone Acetyltransferases and Deacetylases from Chromatin. Journal of Biological Chemistry . 2001 Oct 12;276(41):38307–19.
48. Corpet A. A histone code for the DNA damage response in mammalian cells? 2009;28(13):1828–30.
49. Cimini D, Mattiuzzo M, Torosantucci L, Degrassi F. Histone hyperacetylation in mitosis prevents sister chromatid separation and produces chromosome segregation defects. Molecular biology of the cell. 2003/06/13. 2003 Sep;14(9):3821–33.
50. Li Y, Kao GD, Garcia BA, Shabanowitz J, Hunt DF, Qin J, et al. A novel histone deacetylase pathway regulates mitosis by modulating Aurora B kinase activity. Genes & Development . 2006 Sep 15;20(18):2566–79.
51. Murnion ME, Adams RR, Callister DM, Allis CD, Earnshaw WC, Swedlow JR. Chromatin-associated Protein Phosphatase 1 Regulates Aurora-B and Histone H3 Phosphorylation. Journal of Biological Chemistry . 2001 Jul 13;276(28):26656–65.
52. McCoy CE, Campbell DG, Deak M, Bloomberg GB, Arthur JSC. MSK1 activity is controlled by multiple phosphorylation sites. The Biochemical journal. 2005 Apr 15;387(Pt 2):507–17.
53. Qian J, Lesage B, Beullens M, Van Eynde A, Bollen M. PP1/Repo-Man Dephosphorylates Mitotic Histone H3 at T3 and Regulates Chromosomal Aurora B Targeting. Current Biology. 2011;21(9):766–73.
54. Vagnarelli P, Ribeiro S, Sennels L, Sanchez-Pulido L, de Lima Alves F, Verheyen T, et al. Repo-Man Coordinates Chromosomal Reorganization with Nuclear Envelope Reassembly during Mitotic Exit. Developmental Cell. 2011;21(2):328–42.
55. Castellano-Pozo M, Santos-Pereira JM, Rondón AG, Barroso S, Andújar E, Pérez-Alegre M, et al. R Loops Are Linked to Histone H3 S10 Phosphorylation and Chromatin Condensation. Molecular Cell. 2013;52(4):583–90.
56. Clouaire T, Rocher V, Lashgari A, Arnould C, Aguirrebengoa M, Biernacka A, et al. Comprehensive Mapping of Histone Modifications at DNA Double-Strand Breaks Deciphers Repair Pathway Chromatin Signatures. Molecular Cell. 2018;72(2):250–262.e6.
57. Jackman J, O'Connor PM. Methods for Synchronizing Cells at Specific Stages of the Cell Cycle. Current Protocols in Cell Biology. 1998 Oct 1;0(1):8.3.1-8.3.20.
58. Schorl C, Sedivy JM. Analysis of cell cycle phases and progression in cultured mammalian cells. Methods (San Diego, Calif). 2007 Feb;41(2):143–50.
59. Franken NAP, Rodermond HM, Stap J, Haveman J, van Bree C. Clonogenic assay of cells in vitro. Nature Protocols. 2006 Dec 21;1:2315.

Tables

Table 1 – List of antibodies used in the study

S.No	Protein/PTM	Catalogue no.	Company	Dilution	Purpose
1.	Histone H3	05-499	Millipore	1:2000	Western Blotting
2.	H3K9ac	06-599	Millipore	1:1500 1:250	Western Blotting Immuno-fluorescence
3.	H3S28p	5169	Abcam	1:2000 1:200	Western Blotting Immuno-fluorescence
4.	H3S10p	06-570	Millipore	1:2000 1:200 1µg/100µg chromatin	Western Blotting Immuno-fluorescence Immuno-precipitation
5.	γH2AX	05-636	Millipore	1:5000 1:50 1µg/100µg chromatin	Western Blotting Immuno-fluorescence Immuno-precipitation
6.	PP1α	07-273	Millipore	1:4000	Western Blotting
7.	MKP-1	SC-370	Santa Cruz	1:3000	Western Blotting
8.	Msk1	99412	Abcam	1:1000	Western Blotting
9.	Msk2	99411	Abcam	1:2000	Western Blotting
10.	Beta actin	A-5316	Sigma	1:10000	Western Blotting
11.	α-tubulin	Ab-7291	Abcam	1:200	Immuno-fluorescence
12.	Lamin A	Ab26300	Abcam	1:250	Immuno-fluorescence

13.	Cyclin B	CB-69	Laboratory produced	1:50	Western blotting
14.	p53	(DO-1) sc-126	Santa Cruz	1:1000	Western blotting

Table 2 – List of primers used in the study

Gene name	Forward primer (5-3)	Reverse primer (5-3)
AURKB	TGGACCTAAAGTTCCCCGCT	ACCCGAGTGAATGACAGGGA
MSK1	TTCAGCTGTAAGCCACATGC	TGAGATTGGAAGGGAACCTG
MKP-1	GAGCTGTGCAGCAAACAGTC	ACCCCTTCCTCCAGCATTCTT
PPP1CA	TGCTGGAAGTGCAGGGC	GAAGGTCGTAGTACTGGCCG

Figures

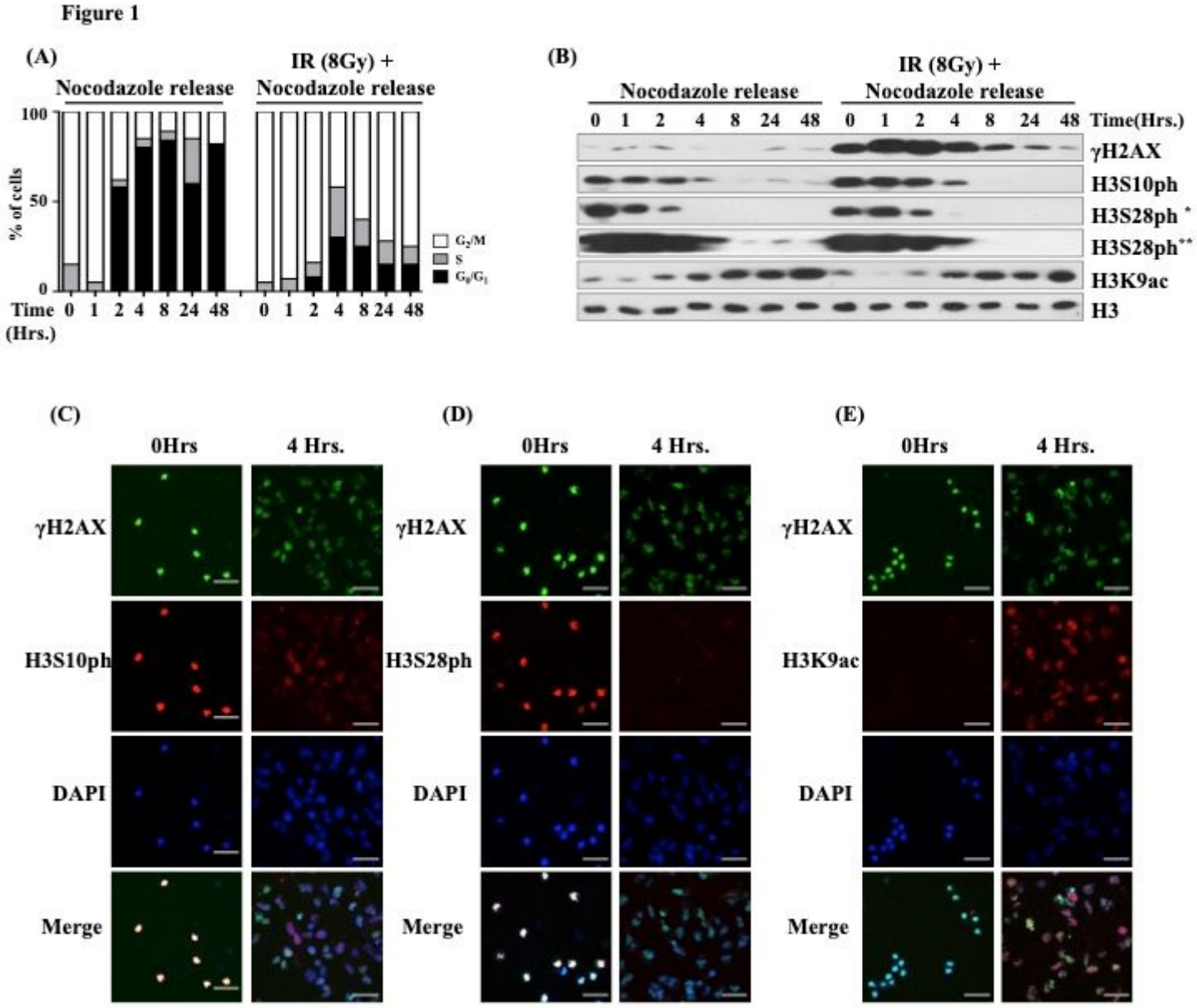

Figure 1

Cell cycle and histone PTM alterations upon mitotic DNA damage. (A) Graph depicting the cell cycle profile of MCF7 cells as analyzed by flow cytometry. (B) Western blots of acid extracted histones against γH2AX, H3S10ph, H3S28ph and H3K9ac at specified time points. Histone H3 serves as loading control. (C) Representative z-stack projection images for co-immunofluorescence of γH2AX with H3S10ph, (D) H3S28ph and (E) H3K9ac at indicated time points. 0 hours represents cells in mitosis and 4 hours represents cells after nocodazole release. Scale bar for each image is 10μm. DAPI staining depicts nucleus. * Represents low exposure, ** represents high exposure, Hrs.- Hours and Gy- Gray.

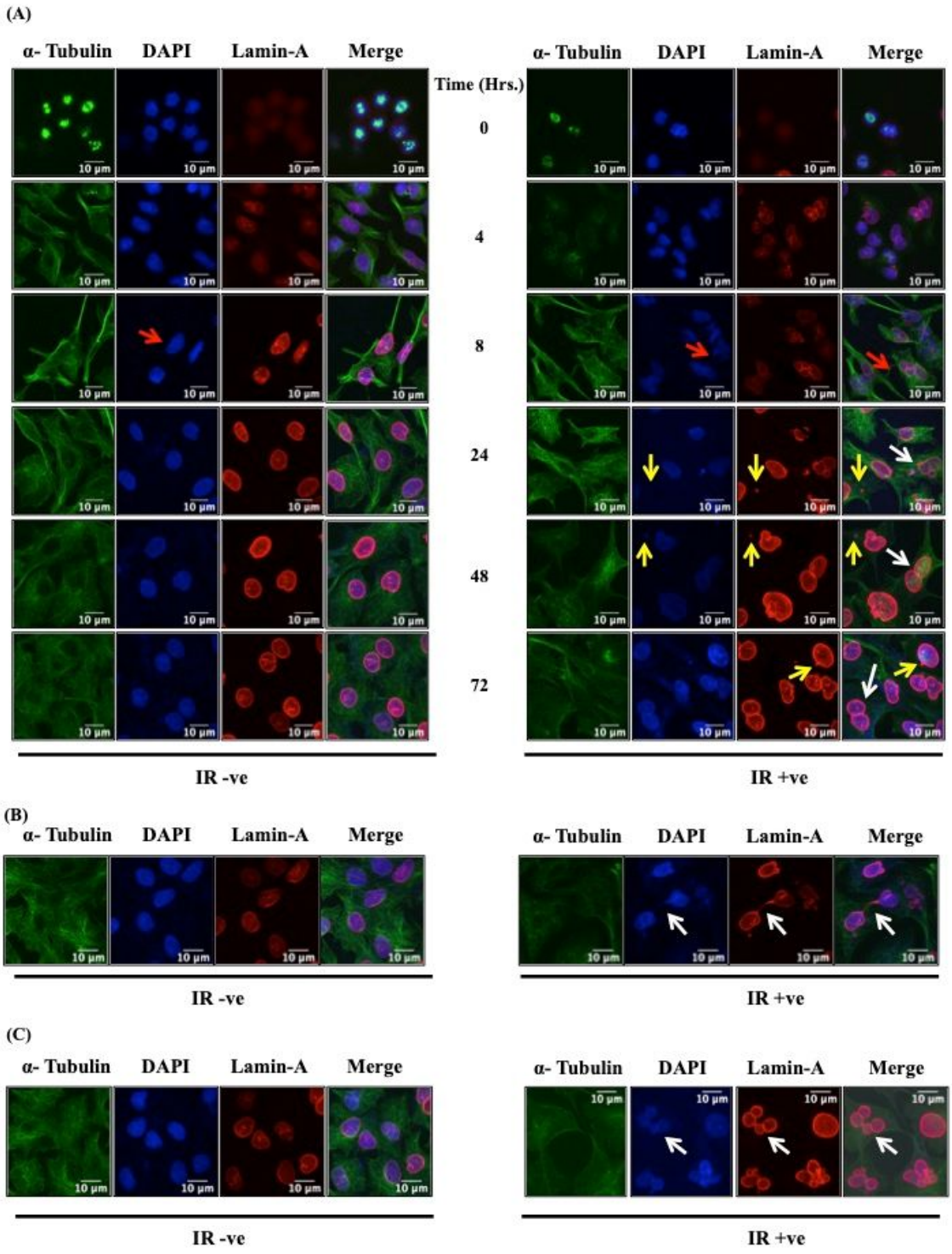

Figure 2

Altered cellular and nuclear morphological features of cells post-mitotic radiation and cell cycle progression. (A) Representative z-stack images of non-radiated (left panel) and radiated (right panel) cells at specific time points post nocodazole release. α- tubulin acts as a marker for individual cells, Lamin-A marks the nuclear boundary and DAPI staining depicts nucleus for all images. Red arrows indicate overall

ated cells. White arrows depict presence of bi-nucleated cells

and yellow arrows depict presence of micronuclei. (B) White arrow depicts formation of chromatin bridge in the radiated cells at time point 4 hours after radiation and mitotic progression. (C) White arrows point to formation of “grape phenotype” nuclei upon radiation exposure at time point 72 hours post radiation and nocodazole release. Scale bar for all images is 10μm. Hrs. – Hours and radiation dose is 8Gy for all samples.

Figure 3

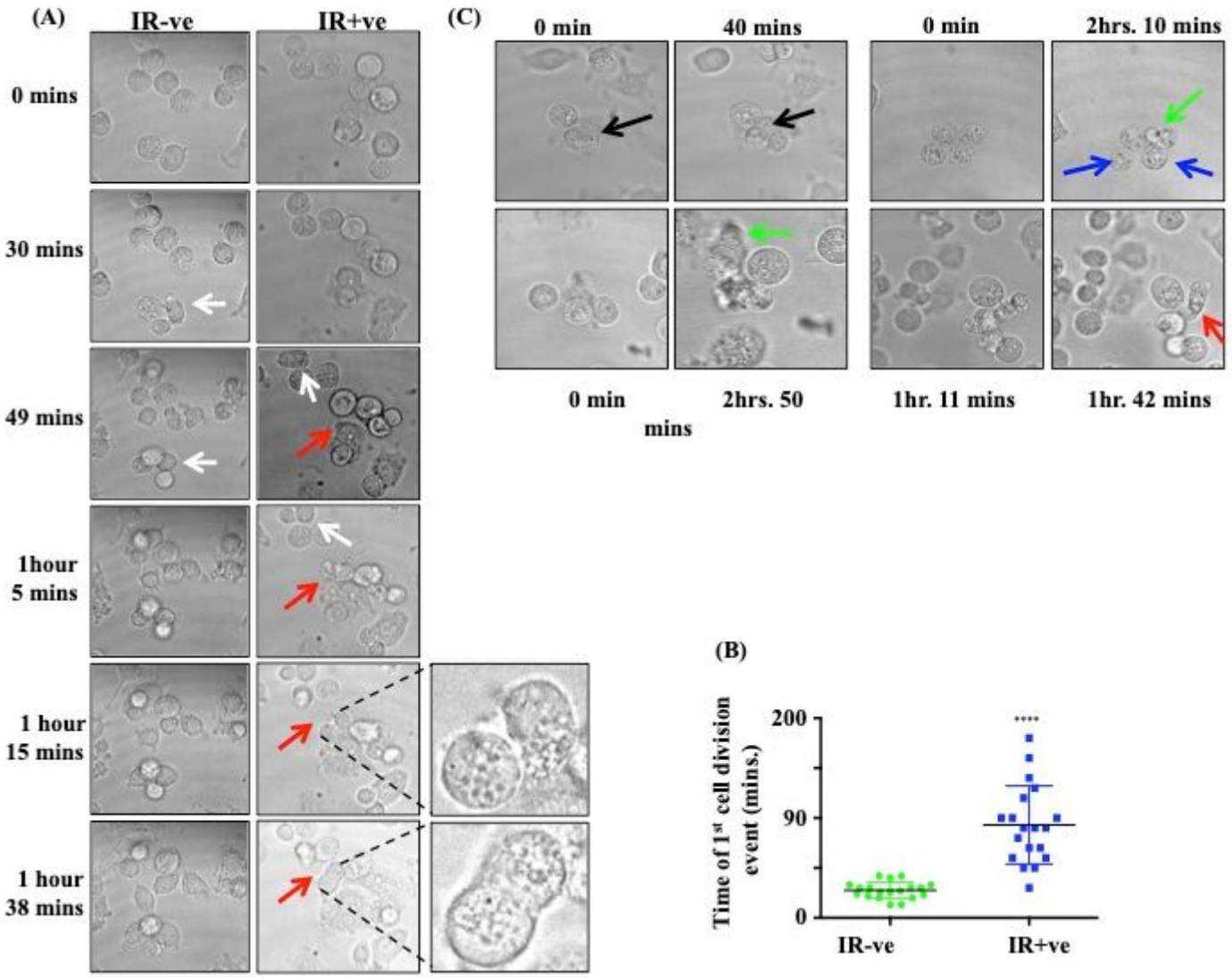

Figure 3

Mitotic radiation-associated cell division defects. (A) Representative images depicting induction of first cell division event for both radiated and non-radiated cells (indicated by white arrows). Red arrows depict cells that divided but ultimately underwent fusion of daughter cells (zoomed out images). (B) Graph representing of time of initiation of first cell division event. Cells counted within 27 different fields from n=3 experiments. (C) Images showing cell phenotypes that arise after radiation of mitotic cells. Black arrows indicate mitotic cells that divide into two daughter cells. Green arrows point to cells that show e arrows depict cells that did not initiate cell division and red

arrows indicate daughter cell fusion. Mins- Minutes. Statistical analysis was performed using unpaired t-test. **** p<0.0001, *** p<0.001, ** p<0.01, * p<0.05 and p>0.05 is considered non-significant.

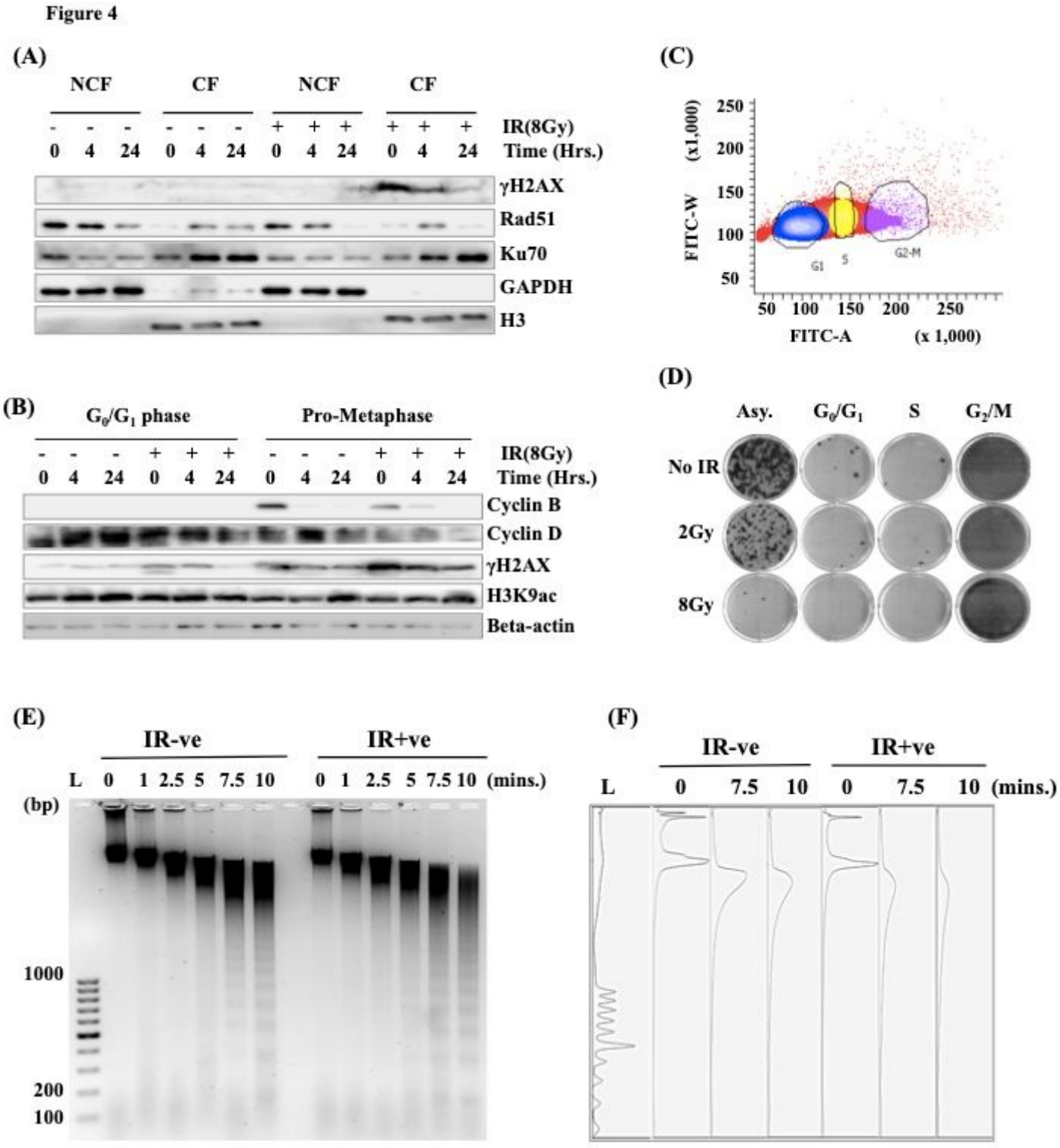

Figure 4

Cell cycle, chromatin and cell survival associated alterations in cell population generated after mitotic DNA damage. (A) Western blots depict levels and localization of DNA repair proteins Ku70 and Rad51 in [illegible] fraction (CF) of mitotic cells with and without radiation, at

indicated time points. GAPDH and Histone H3 serve as loading controls for nucleocytoplasmic fraction and chromatin fraction, respectively. (B) Western blots for Cyclin B, Cyclin D and histone PTMs γH2AX, H3S10ph, H3S28ph and H3K9ac from total cell lysates of cells synchronized in G0/G1 and mitotic phase of cell cycle at specified time points, with and without radiation. Beta-actin serves as loading control. (C) Graph represents the ploidy parameters used for Fluorescence Activated Cell Sorting (FACS) based separation of G0/G1 (2N), S (2N-4N) and G2/M (4N) cell cycle phases in a population obtained 48 hours after nocodazole release and mitotic progression of radiated M-phase cells. X-Axis represents fluorescence intensity and Y-Axis represents number of cells (x1000). (D) Clonogenic assay representing reduction in overall survival of the FACS sorted cell populations compared to an asynchronous population, upon radiation exposure. (E) TAE-Agarose gel based representation for MNase digestion of non-radiated and radiated cells 48 hours after nocodazole release and (F) densitometric representation of the same. Time indicates incubation time of nuclei with MNase. Black arrows represent alterations in chromatin architecture. Gy- Gray, Asynch- Asynchronous, L - 100 base pair ladder, b.p.- base pair and Hrs. - Hours. Radiation dose is 8Gy for all samples. Kindly note that western blots depicted separately in Fig. 4A and 7D were a part of the same experiment but are depicted as separate figures. They are derived from the same experimental nucleo-cytoplasmic and chromatin lysates; hence have same histone H3 and GAPDH loading control blots.

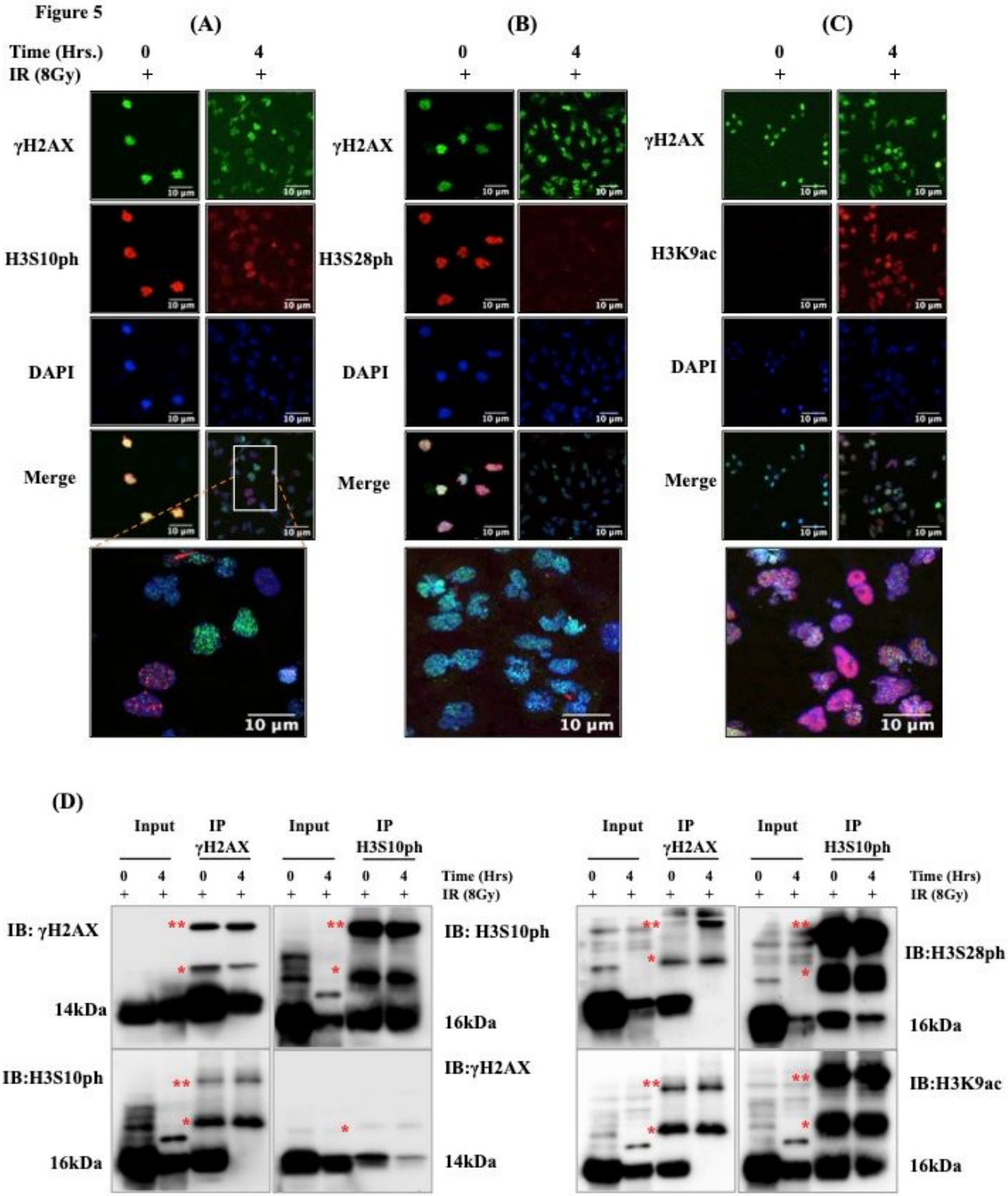

Figure 5

Co-localization analysis of γH2AX with H3S10/28ph and H3K9ac during mitotic DNA damage response. Representative z-stack images for co-immunofluorescence based co-localization analysis of γH2AX with (A) H3S10ph, (B) H3S28ph and (C) H3K9ac at specified time points after radiation and nocodazole release. Time points 0 hour depicts time when cells were still in mitosis and 4 hours denotes time elapsed t shows zoom-out image at 4 hour time point. Yellow color

denotes co-localization of indicated histone marks. DAPI acts as nuclear marker for all images (D) Mono-nucleosomal immuno-precipitation (IP) performed with anti-γH2AX and anti-H3S10ph antibody at the indicated time points after radiation and nocodazole release. Immuno-blotting (IB) performed with anti-γH2AX, anti-H3S10ph, anti-H3S28ph and anti-H3K9ac antibodies. Input is 10% amount of mononucleosomes used for immuno-precipitation. * and ** denote antibody heavy chain (55kDa) and light chain (25kDa) of the antibodies, respectively. Hrs. – Hours and Gy- Gray. Scale bar for all microscope-based images is 10μm. Radiation dose is 8Gy for all samples.

Figure 6

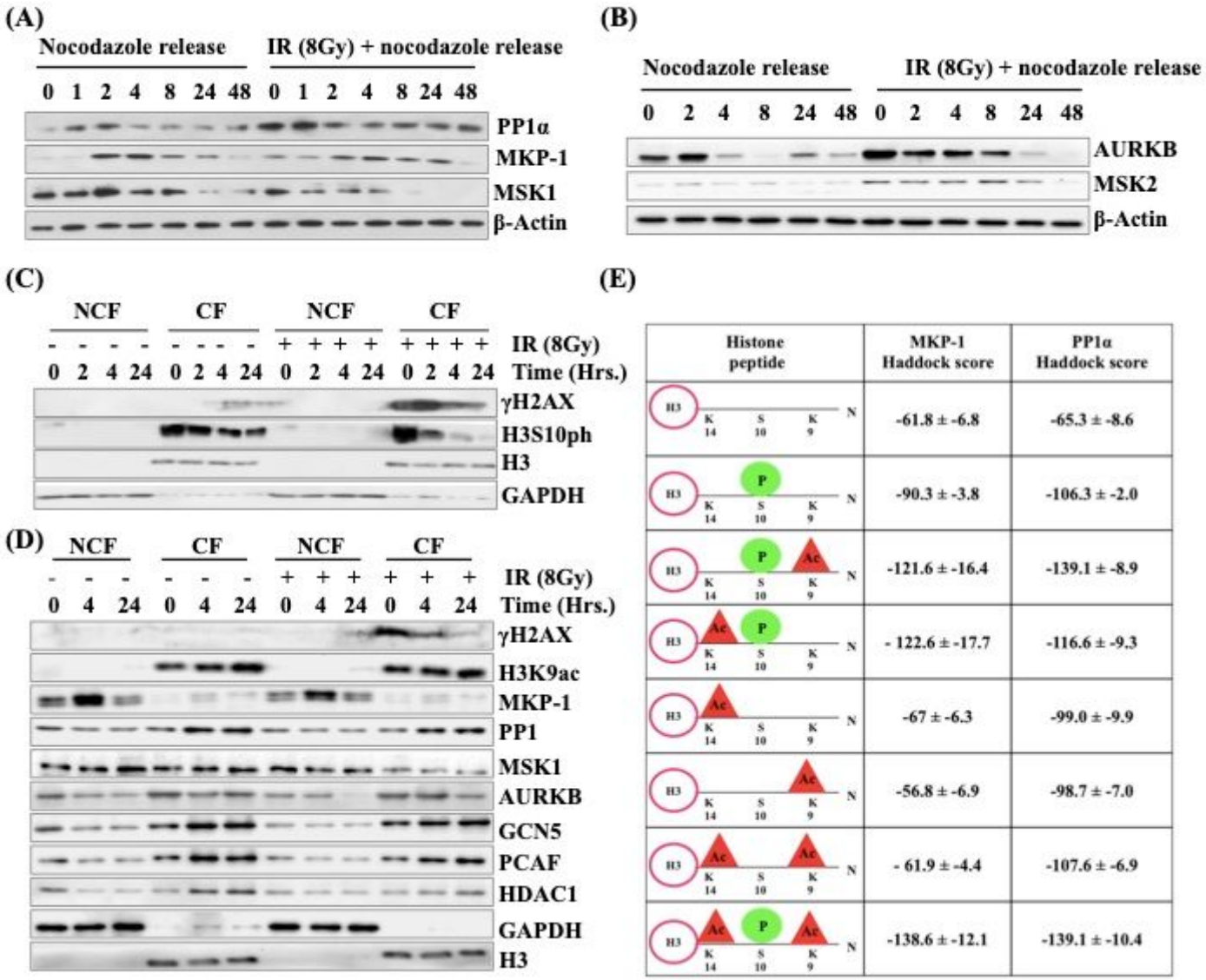

Figure 6

Alterations of histone modifying enzymes during mitotic DNA damage. Western blots depicting levels of chromatin modifying enzymes (A) PP1α, MKP-1, MSK1 and (B) MSK2 and AURKB from total cell lysates. Beta actin serves as loading control for both (A) and (B). (C) Western blots of histone PTMs γH2AX, H3S10ph, H3S28ph and H3K9ac and (D) γH2AX, H3S10ph, H3S28ph and H3K9ac chromatin modifying [illegible] erases at specified time points in nucleocytoplasmic fraction

(NCF) and chromatin fraction (CF). GAPDH and H3 serve as loading controls for NCF and CF, respectively. (E) Molecular modelling for MKP1 and PP1α with different sets of H3 peptides (having a combination of PTMs H3S10ph, H3K9ac and H3K14ac). Haddock score depicts affinity of interaction of particular phosphatase and histone PTM combination. Hrs.- Hours, Gy- Gray. Kindly note that western blots depicted separately in Fig. 4A and 7D were a part of the same experiment but are depicted as separate figures. They are derived from the same experimental nucleo-cytoplasmic and chromatin lysates; hence have same histone H3 and GAPDH loading control blots.

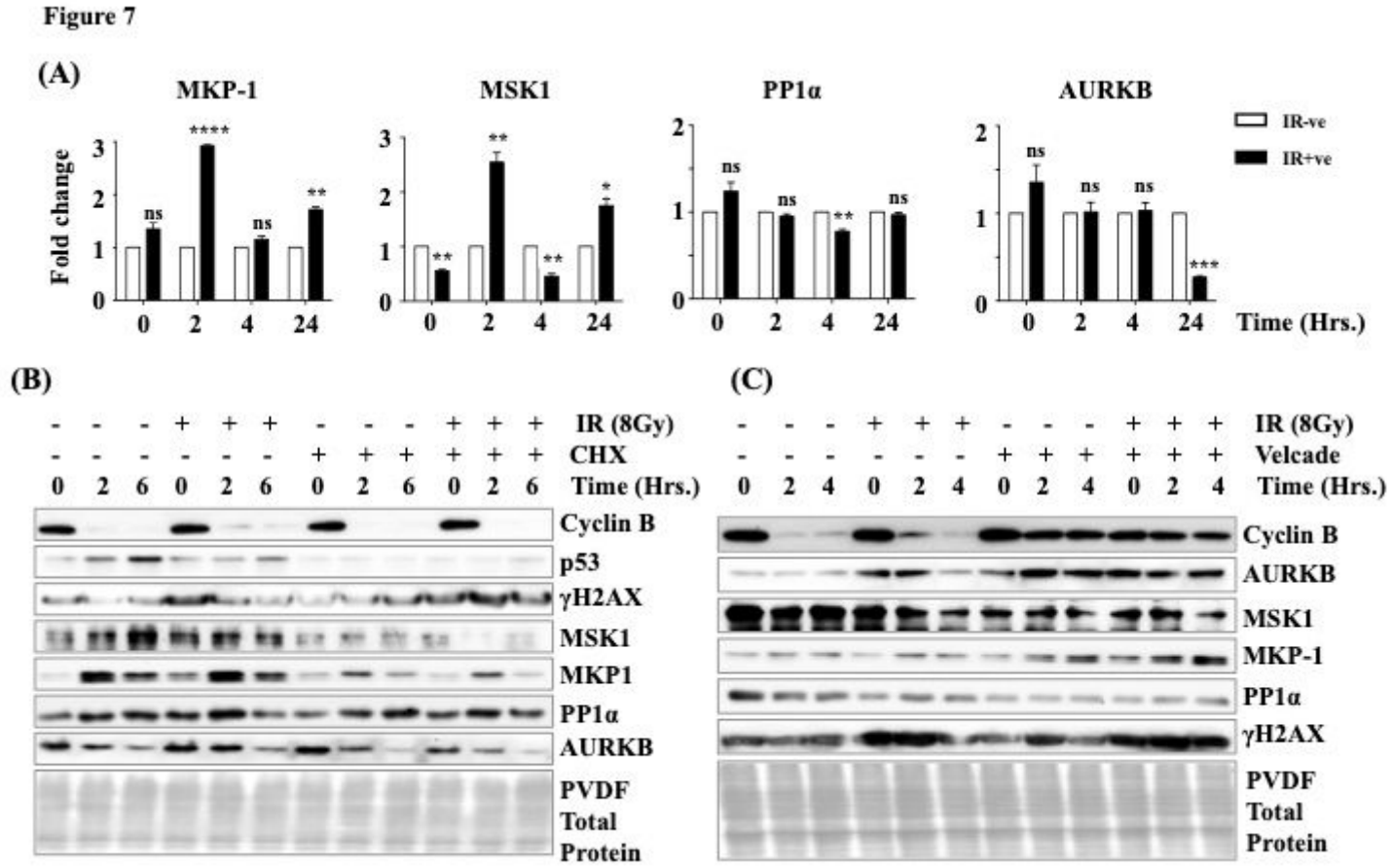

Figure 7

Regulation of histone modifying kinases and phosphatases in response to mitotic DNA damage. (A) Graphs depict real-time PCR based analysis of transcript levels of MKP-1, PP1α, MSK1 and AURKB at specific time points after radiation and nocodazole release, represented as fold change. Values normalized to non-radiated control of each time point, represented as fold change equal to 1. (B) Western blots depict levels of MKP1, PP1, MSK1 and AURKB in total cell lysates prepared from cycloheximide (50μg/ml) treated and (C) proteasome inhibitor velcade (1μM/ml) treated mitotic cells at specified time points. PVDF membrane serves as loading control. Statistical analysis was performed using unpaired t-test. **** $p<0.0001$, *** $p<0.001$, ** $p<0.01$, * $p<0.05$ and $p>0.05$ is considered non-significant. n.s – non-significant. Hrs. – Hours.

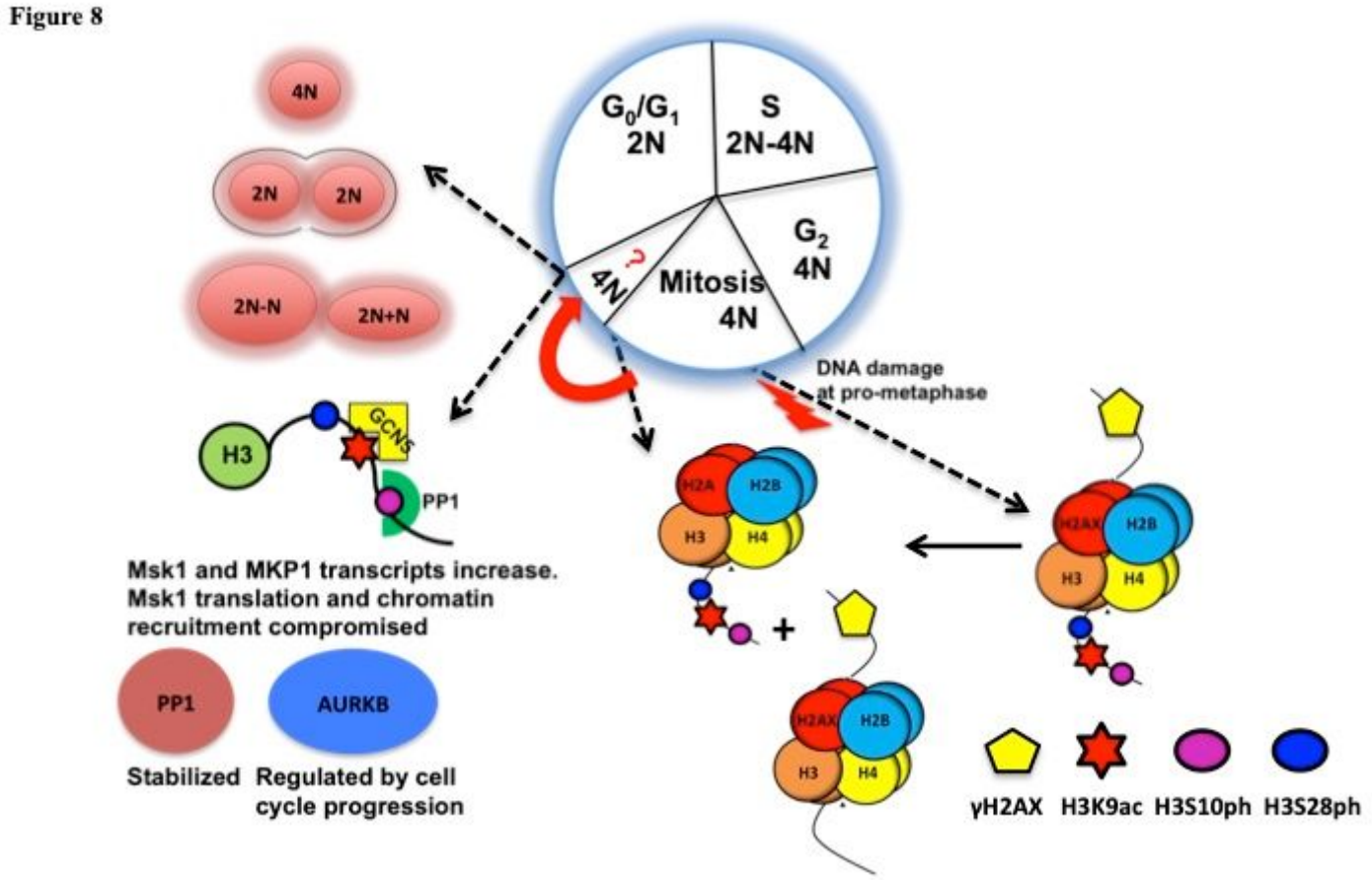

Figure 8

Model depicting scenario during mitotic DDR. The cartoon represents the cellular and epigenetic changes that occur during mitotic DDR and after these cells resume cell cycle progression.

Supplementary Files

This is a list of supplementary files associated with this preprint. Click to download.

- AdditionalFile3.tiff
- AdditionalFile2.tiff
- AdditionalFile1.tiff